**Performance of integrated thin film silicon solar cell based water splitting devices under varying illumination angle and an estimation of their annual hydrogen production**

Katharina Welter[1], Jan-Philipp Becker[1,2], Friedhelm Finger[1], Wolfram Jaegermann[3]and Vladimir Smirnov[1]

1 IEK-5 Photovoltaik, Forschungszentrum Jülich GmbH, D-52425 Jülich, Germany
2 now at: Zentrum für Sonnenenergie und Wasserstoff-Forschung Baden-Württemberg, D-70563, Stuttgart, Germany
3 Institute of Material Science, TU Darmstadt, D-64287 Darmstadt, Germany

**Abstract**

We have investigated the influence of simulated outdoor illumination conditions on the functionality of photovoltaic-biased electrosynthetic (PV-EC) systems used for the production of hydrogen as a renewable and storable fuel via solar water splitting. Thin film multi-junction solar cells were adopted for the PV part of the device together with an electrosynthetic cell with a Pt/$IrO_x$ catalyst pair in 1 molar potassium hydroxide electrolyte solution. We studied the influence of the incident illumination angle on the solar-to-hydrogen efficiency and we give a first evaluation of the long term (1 year) performance of PV-EC systems in terms of hydrogen volume produced for a given geographical location. In this approach variations from the standard AM1.5 G type illumination expressed as changes in the average photon energy of the spectra are used to simulate different geographical locations as well as seasonal and daily changes in the illumination spectra. Finally, we compare the impact of various types of multi-junction photovoltaic devices (tandem, triple and quadruple junctions) on the annual solar hydrogen production.

**Introduction**

Hydrogen attracts significant attention as a storable carbon-free fuel which can be obtained via solar water splitting utilizing photovoltaic-biased electrosynthetic (PV-EC) systems.[1] In this device, a solar cell (PV) is directly combined with an electrochemical cell (EC).[2,3] In order to drive the spontaneous water splitting reaction, the voltage generated by the photovoltaic cell has to exceed 1.23 V (thermodynamic potential) plus overpotential losses occurring in the system.[4] Photovoltaic multijunction and tandem solar cells can generate sufficient photovoltage to drive the electrochemical reaction and various configurations of the multijunction systems have been reported recently [5-7 ,8, 9, 10] . Multi-junction silicon solar cells can provide photovoltages in the range of 1.5 – 2.8 V, demonstrate good stability under prolonged illumination [11] as well as reasonably high photocurrent densities, depending on the amount of series connected sub cells and the corresponding band gaps of the absorber material.[5–7] The performance of photovoltaic cells as well as PV-EC devices are usually evaluated under the standard test conditions (STC: 25°C, 1kW/m² (1 sun) illumination intensity of the AM 1.5 G spectrum under 0° incident illumination angle).[12–14]These test conditions significantly differ from the existing various outdoor conditions and spectral compositions, for example, because of seasonal and daily variations in the incident sun spectrum.[11–15]

The PV devices have been studied under artificial and original field conditions extensively [15,17,18,20–22], however detailed works on integrated PV-EC devices have not been performed systematically yet.[23–25]

Here, it is necessary to highlight that one cannot conclude on the performance of integrated PV-EC devices simply from the available data of various PV systems. We point out two important reasons for that:

- In the case of a photovoltaic device it is possible to draw power at all points of the illuminated current-voltage curve of the device. This is valid for any various irradiations under condition that the product $|J|\cdot V\cdot FF$ is above zero. In contrast, for the case of an integrated PV-EC system the production of hydrogen could only take place for output voltages exceeding a particular number which is a sum of the thermodynamic potential and additional losses in the system. Therefore, the variations in the illumination that alter the current-voltage characteristic of the integrated system in the way that the value *V* at the operation point is insufficient, will stop the generation of the hydrogen (see Figure 1 for illustration). This will result in additional considerations for the case of realistic applications, for example, an implementation of additional electronic control or power back-up units may be needed.

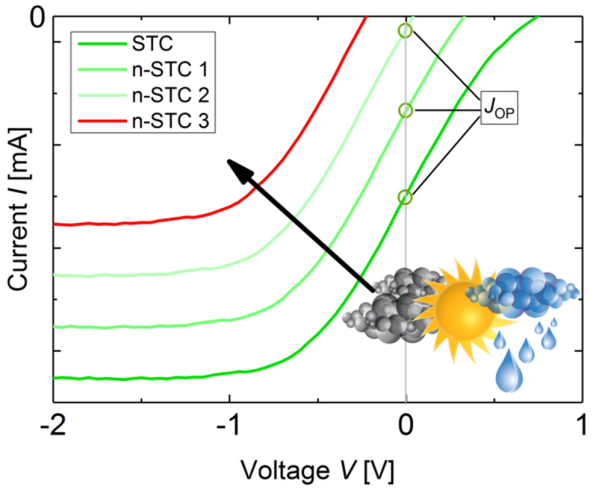


Figure 1: Schematic illustration of the possible influence of varying outdoor conditions (STC and n-STC stands for standard and non-standard test conditions, respectively) on the J-V curves of the PV-EC devices operating without additional bias. In the case of the green curves, hydrogen can be generated since an operating current can be extracted. For the red curve, no current could be extracted at 0V point, and consequently the generation of hydrogen is not taking place.

- In realistic field operation cases with notable changes in temperature, also affected by the changes in the illumination spectra and also day-night cycling can bring an influence on the functionality of the electrochemical components of the integrated system. This may have positive or negative effects on the device functionality and hydrogen production. Thus it is necessary to investigate these aspects on the integrated PV-EC devices also[23,24].

We recently reported on the performance of PV-EC systems based on triple junction silicon solar cells under varied illumination states, such as red or blue shifted spectra[24], as well as varied illumination intensity[24,25] and operation temperatures.[24,25] In the present study, we elaborate on these investigations including studies under different illumination angles and estimations of the annual hydrogen production from combined PV-EC systems considering illumination spectra variations due to geographical situation of an installed solar water splitting system.

At first, we investigated the effects of the incident illumination angle on the performance of PV-EC systems. The angle of illumination changes along the day and year and is also defined by the

geographical location (latitude). For example, in Bavaria (Germany), the variation in the illumination angle at midday time between June and December is close to 47° (the angle is 65.3° on 21.06 and 18.5° on 21.12). A change in illumination angle leads to a reduced number of incident photons per area, if the device position is static. We evaluated the *J-V* behavior of a multi-junction silicon solar cell under varying illumination angles and combined them in an electrical series model[26,27,29] with the respective linear sweep voltammetry curves, to predict the performance of the combined PV-EC systems under varying incident angles. The results under varying angles (static device position) are compared to the performance for the case that the device position is adjusted constantly such that the effective illuminated area is constant. Contrary to the measurement of PV-EC devices under laboratory conditions, where the device is usually set in a horizontal or vertical position, for the outdoor application PV-EC devices are usually installed in a tilted position, which has to be additionally considered regarding the device design.

Secondly, to estimate the annual hydrogen production of a combined PV-EC system we focus on the variation in the spectral composition of the illumination as determined by geographical location together with annual variation. We describe the steps to evaluate the annual functionality of the combined PV-EC systems depending on the average photon energy of the incident spectra. The average photon energy (APE) describes the quality of an illumination spectrum and is defined as the total energy in a spectrum (spectral irradiance) divided by the photon flux density (total number of photons in the spectrum)[28]. High APE values describe blue rich spectra (e.g. in summer) and low APE values stand for red shifted spectra (e.g. in winter)[16,18].
Finally, we compare hydrogen production of combined PV-EC systems with tandem, triple or quadruple junctions, respectively in view of the additional gain from higher output voltage devices compared with the complexity of the preparation process of multi-junction solar cells.

**Experimental Section**

Integrated PV-biased electrosynthetic cell

An integrated photovoltaic-biased electrosyntheticcell (PV-EC) consists of a solar cell (PV), which is closely connected to an electrolysis cell (EC). Herein, the PV cell is used as part of the working electrode. In our device the hydrogen evolution reaction (HER) takes places on a sheet metal electrode connected to the rear side of the PV device. Depending on the composition and properties, the sheet metal electrode can serve as HER catalyst itself or respective HER catalysts can be deposited on the surface that is directly in contact with the electrolyte, which is in most cases 1 M potassium hydroxide or 1 M sulfuric acid. In this device, the illuminated solar cell area and the area of contact with the electrolyte are equal (0.5 cm² in both cases). In Figure 2 a schematic of a PV-EC device is shown which utilizes a triple junction silicon solar cell with two amorphous hydrogenated silicon (a-Si:H) sub cells and one microcrystalline hydrogenated silicon (µc-Si:H) sub cell (a-Si:H/a-Si:H/µc-Si:H).[5]

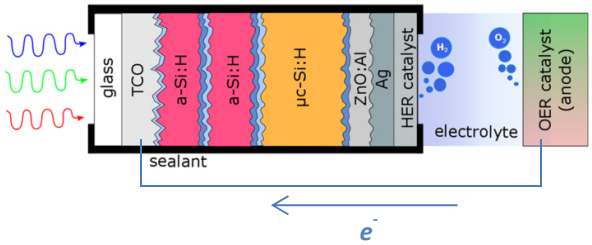


Figure2: Schematic of a combined PV-EC system utilizing an a-Si:H/a-Si:H/µc-Si:H triple junction solar cell.

For these PV-EC systems, the current-voltage behavior, expressed by the voltage $V_{PV\text{-}EC}(j,T)$ in dependence on $j$ and temperature $T$, can be described by using an equivalent circuit model with electrically contacted independently evaluated $J$-$V$ parameters ($V_{PV}(j,T)$ and $V_{EC}(j,T)$) at a respective temperature:[26,27,29]

$$V_{PV-EC}(j,T) = V_{PV}(j,T) + V_{EC}(j,T) \quad [1]$$

Therefore, the J-V characteristics of the PV device under different incident angles and different illumination spectra respectively can be combined with the current-voltage behavior of the electrolysis to investigate the $JV$ behavior of the integrated device under different illumination angles and under various average photon energy spectra respectively. The solar-to-hydrogen ($\eta_{STH}$) efficiency can be extracted from the $JV$ curve $V_{PV-EC}(j,T)$ at bias free operation conditions ($V$=0V). It is calculated using the following equation:

$$\eta_{STH} = \frac{power\ out}{power\ in} = \frac{\Delta E \times \eta_F \times j_{OP}}{total\ integrated\ power\ input\ density} \quad [2]$$

The thermodynamic potential $\Delta E$ in case of the water electrolysis is equal to 1.23 V, $\eta_F$ describes the Faradaic efficiency, that is considered to be 1 based on earlier measurements[5]. Note however, that in the present study, only the effects of changes in the illumination conditions and corresponding tendencies are discussed and possible related changes in the Faradaic efficiency are so far not considered. $j_{OP}$ is the current density at bias-free conditions (V = 0V), the input power described in denominator stands for the illumination intensity (e.g. 1 kW/m²).

Preparation of the solar cells

The intrinsic and doped silicon-based materials in the solar cells, which were used as current-voltage sources, were prepared in p-i-n deposition sequence via plasma-enhanced chemical vapor deposition. The substrate used for the deposition was $SnO_2$:F coated glass; ZnO:Al/Ag/ZnO:Al was prepared as highly reflective back contact by reactive magnetron sputtering.[30] Further information on the solar cell fabrication can be found elsewhere.[5–7]

Current-voltage (JV) measurements under various incident illumination angles

The J-V characteristics were obtained under varied angles of incident illumination (varied between 0 to 60°) of the standard AM1.5G light source from a class AAA sun simulator (Wacom type WXS-140S). The illumination area of the sun simulator is 10 cm x 10 cm, which is two orders of magnitude the size of the illuminated solar cell area under normal incidence conditions ($A_{0,PV}$=1 cm²). The illumination cases for the J-V system are illustrated schematically in Figure 3. We will describe in the following the effect of an increase in the incident illumination angle using an "effective illuminated area" of the device, which depends on cosine law:

$$A(\alpha) = A_0 \cdot \cos(\alpha) \qquad [3]$$

This approach is similar to a case with a decreased number of photons per solar cell area when angle of incidence $\alpha$ is tilted (see Figure 3).[27,28] Normal incidence corresponds to 0° and 1 sun illumination in all investigated cases.


Figure 3: Schematic illustration of the illumination cases under various incident angles used during the current-voltage (JV) measurements. An overall spot size of 10 cm x 10 cm is illuminated, which is two orders of magnitude the size of the illuminated solar cell area under normal incidence conditions. A variation of the angle leads to a reduced photon flux per unit area (reduced "effective illuminated device area") following the "cosine law" $A(\alpha)=A_0 \cdot \cos(\alpha)$.[31,32]

Current-voltage measurements under various illumination spectra (*JV*):

For the plain AM1.5G spectrum illumination we use a class AAA sun simulator (see above). For realizing different spectral conditions, a combination of several high-output LEDs (465 nm, 850 nm) was adopted. The 465 nm LED was used to enhance the short wavelength range (blue shift), while the 850 nm LED enhanced the wavelength share in the long wavelength range (red shift). Generally, the intensity of the simulated spectrum was unaltered and equal to 1 kW/m². Therefore, the intensity of the AM1.5G source was reduced according to the intensity of the added LED light. Figure S1 exemplarily shows the blue shifted spectrum. Additionally, to generate a wider range of average photon energies (APE), the share of intensities from the two light emitting lamps (xenon and halogen lamps) were altered (e.g. in the case of low APEs, the intensity from the xenon light source was

decreased, while the intensity of the halogen source was enlarged).The quality of the spectra is related to an average photon energy APE given as the ratio of the total energy in a spectrum (irradiance) to the photon flux density (total number of photons in the given spectrum):

$$APE = hc \frac{\int_a^b E_e(\lambda) d\lambda}{\int_a^b \lambda E_e(\lambda) d\lambda} \quad [4]$$

In this equation, *h* is the Planck constant, *c* is the speed of light, $E_e$ is the spectral irradiance and $\lambda$ is the wavelength. The investigated wavelength range is between 300 nm and 1350 nm. The obtained APE range investigated in this study covers a range of ΔE= 0.44eV and is shown relative to the APE of the standard AM1.5G spectrum (corresponding to the actual value of 1.71 eV $APE_{AM1.5G}$ and the relative value ΔAPE of 0 eV). Since the actual APE value may depend on the integration wavelength range (and to an extent on the facilities available in different laboratories), the presentation of the results vs. relative APE makes the approach used in this work easily applicable for a wide range of groups and facilitate better comparison between the results obtained in various laboratories. In order to compare the photovoltaic and the respective combined photovoltaic-electrochemical behavior under various illumination conditions, the total incident power of the spectrum was maintained at 1 kW/m² and is therefore equal to the total incident power under standard test conditions. Please note that in the actual outdoor application a change in APE could take place together with variations in intensity and the total incident power of the illumination spectrum would be decreased, leading to a decreased hydrogen output.

Electrochemical experiments:

The following catalyst pair was used in the present work: Pt for the HER electrode (provided by Goodfellow GmbH, Germany, 99.95% purity) and IrOx for the OER electrode (density of 12 g Ir/m$^2$ on Ni sheet, provided by METAKEM GmbH, Usingen, Germany). The J-V characteristics of the catalysts were studied by linear sweep voltammetry measurements (LSV) conducted at a scanning rate of 50 mV/s in 1M KOH solution at standard temperature ( w/o stirring). Gamry potentiostat type Reference 600 was used.

Evaluation of annual hydrogen generation:

The procedure to calculate of the annual hydrogen production is described below and discussed in more detail in the following section:

1. The J-V characteristics of the entire PV-EC systems were evaluated under both standard AM1.5G illumination and modified illumination conditions (variations in APE) for the intensity of 1 kW/m² (corresponding to 1 sun).
2. The STH values were evaluated for both standard (AM1.5G spectra) and modified illumination conditions (variations in APE) for 1 kW/m² intensity based on J-V characteristics of the PV system in combination with J-V characteristics of the catalyst pair described above. The evaluation of the STH values in each case was based on the electrical series connection model (see description above).
3. As an example of outdoor variations in the realistic spectra, representative reference data describing annual spectral composition for a given location depending on the APE was chosen [18]. To obtain the data of irradiance as a function of APE, the reference data were fitted with a

Gaussian curve from which then individual data points can be taken. Additionally, the reference data (1.05 kW/m²) were normalized to a standard intensity of 1 kW/m².

4. In this step, the STH values evaluated in (2.) can be presented in relation to the particular average photon energy values evaluated in (3.) Then the STH values as a function of the average photon energy were convoluted with the corresponding irradiance for each APE intervals.

5. The convoluted STH values over the studied interval of APE were integrated to obtain the overall value for the given spectral compositions.

6. In the following, the coefficient of 2.5 L/m² (defined from the experiments for the volume of generated hydrogen corresponding to 1% STH[29] ) is multiplied with the values obtained in (5.). The obtained result defines the amount of hydrogen produced for a given spectral data and device. The calculation of the experimentally obtained coefficient of 2.5 L/m² and the theoretically calculated maximum factor of 3.7 L/m² are presented in the supplementary information (see **Error! Reference source not found.** and Figure S3). Figure S3 shows the hydrogen volumes produced using the two different factors.

$$V_{annual}(Hydrogen) = 1\ m^2 \cdot 2.5\ L/m^2 \cdot \int_{APE1}^{APE2} P(APE)\ \cdot\ STH(APE)\ dAPE \qquad [5]$$

**Results and discussion**

***Angular dependent measurements***

Figure 4 shows the values from the J-V characteristics (efficiency $\eta$, open circuit voltage $V_{OC}$, fill factor *FF*, short circuit current density $J_{SC}$, voltage at the maximum power point $V_{MPP}$, and current density at the maximum power point $J_{MPP}$) collected for the a-Si:H/a-Si:H/µc-Si:H solar cell under different incident angles up to 60° (the measured current-voltage characteristics are presented in Figure S4). The data were normalized to the values corresponding to the case of normal incidence 0°. As one can see in Figure 4 the changes in the J-V parameters are related to the changes in the incident photon flux and effective changes in the illumination area (following cosine law [3]).

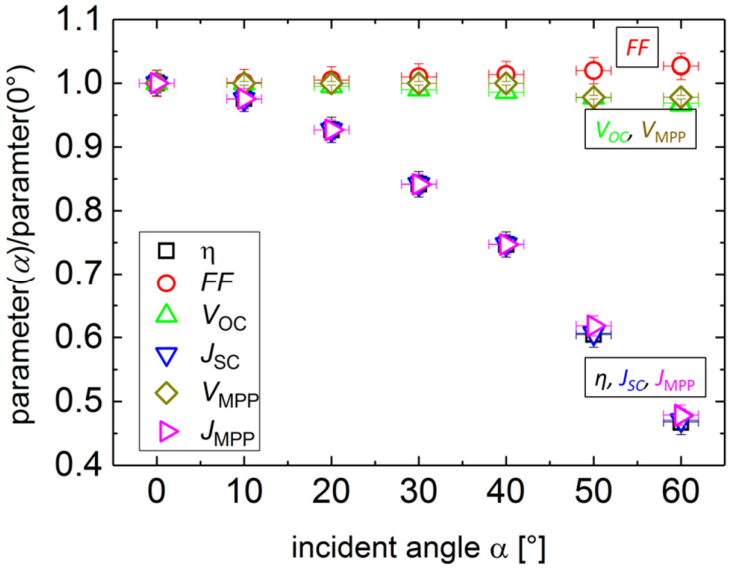

Figure 4: Normalized current-voltage values (efficiency η, open circuit voltage $V_{OC}$, fill factor FF, short circuit current density $J_{SC}$, voltage at the maximum power point $V_{MPP}$, and current density at the maximum power point $J_{MPP}$) as a function of the incident angle (area correction was not applied in all cases).

It can be seen that both $V_{OC}$ (emerald points) and $V_{MPP}$ (rhombuses) are slightly reduced with increasing angle. The trend in *FF* (red circles) shows only little raise upon changes in the angle between 0° to 60°. In contrast, significant changes are observed for $J_{SC}$ (blue triangles) and $J_{MPP}$ (magenta triangles)) . It is evident in Figure 4 that both these parameters follow the same trend and are decreased down to 0.5 from the value of 1 corresponding to the normal incidence. A similar tendency is observed for $\eta$ (square points) which reduced to about one half upon changes in the angle between 0° to 60°. In the case of a static device position which results in a reduced illumination intensity[24,25], the decrease of $J_{SC}$ can be related to the decreased amount of photons absorbed by the photovoltaic device. On the other hand, changes in $V_{OC}$ are directly related to the splitting of the quasi-Fermi level under illumination.[34,35] An here observed slight improvement in fill factor (*FF*) values upon changes in the angle between 0° to 60° has an analogous origin to the effects of decreased photon flux on the solar cell performance [20,24]. These effects are usually related to the distribution of the field in the solar cell upon illumination and a lower recombination rate of electron-hole pairs in the active layer of the solar cell.[36,37] Note that here an improvement in the built-in field brings no positive effect on $V_{OC}$, which is dictated by the reduced number of the photogenerated electron hole pair and consequently reduced quasi-Fermi level splitting with an increasing angle.

To compare the functionality for the PV-EC system in static or adjusted position and to identify the influence of the effective illuminated area, the current densities were corrected according to cosine law and compared to the initially measured values. The values of $J_{SC}$ and $J_{MPP}$ (black and red points, respectively) are plotted in Figure 5 for two cases: corrected following cosine law and actual measured values (no correction applied). The data are shown as a function of incident angle up to 60°. After adjusting the area following cosine law [3], $J_{mpp}$ is reduced from around 6.3 mA/cm² down to around 6 mA/cm² (corresponding to a reduction of some 5 %) over the range of angles investigated. The observed decrease in $J_{SC}$ is around 6 % down to a value of 6.6 mA/cm². The decrease in current density of ~5% obtained after performing the area correction could probably be related to optical losses taking place in the stack e.g. at the interfaces between air and glass substrate and also between various silicon thin films, as reported in literature[32]. Overall, Figure 5 shows that the performance reduction observed in Figure 4 is mostly due to the static device position and therefore to the reduced effective illuminated device area. Possible optical losses play a minor role.

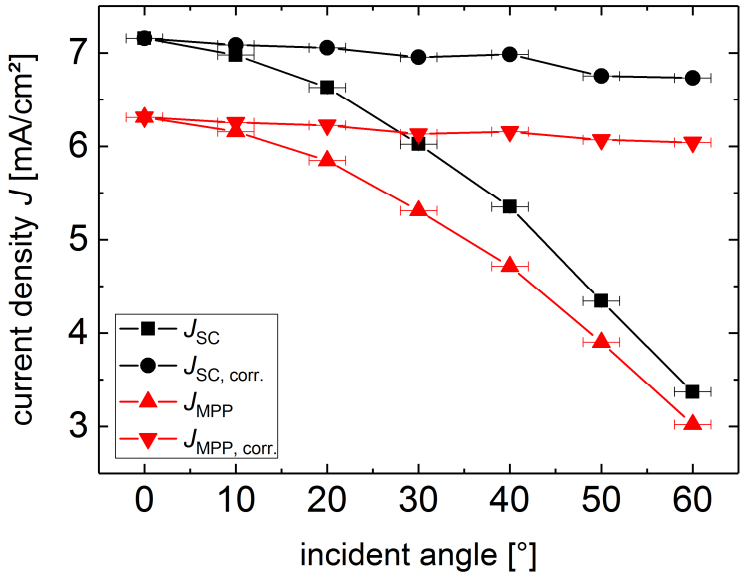


Figure 5: Current densities $J_{SC}$ and $J_{MPP}$ plotted as a function of illumination angle. Black cycles and red upsidedown triangles represent the case when the area was corrected (see details in text).

*Evaluation of the STH efficiency $\eta_{STH}$ under various incident illumination angles*

In the following, the influence of incident angles on the performance of the PV-EC system was studied. Due to the electrical series connection, the J-V characteristics obtained for the catalytic system (Pt and $IrO_x$) were joined with J-V curves of the photovoltaic system (see Figure S4) to obtain the operating point of the integrated device (corresponding to 0V condition).[27,29,38] Then the STH efficiency $\eta_{STH}$ can be evaluated following eq. [2]. The modeled J-V characteristics of the entire photovoltaic-electrochemical system under illumination are plotted in Figure S-5).

To illustrate the influences of the static device position and therefore the influence of the illumination area on the functionality of the system, Figure 6 summarizes the $J_{OP}$ and the STH values. The data are presented for the illumination angles varied between 0° to 60°. In the case of the data when area correction was made, the $J_{OP}$ and STH values are only slightly reduced, likely due to the presence of optical effects at the interfaces as pointed out earlier. In the other case (no area adjustment), the $J_{OP}$ is significantly reduced from around 6.7 mA/cm² down to around 3.2 mA/cm² over the range of investigated angles. The reduction in the operation current density, in turn, results in the decrease in the STH efficiency $\eta_{STH}$, roughly by half down to almost 4% at the maximum incident angle value of 60°, which also reduces the amount of H2 produced.

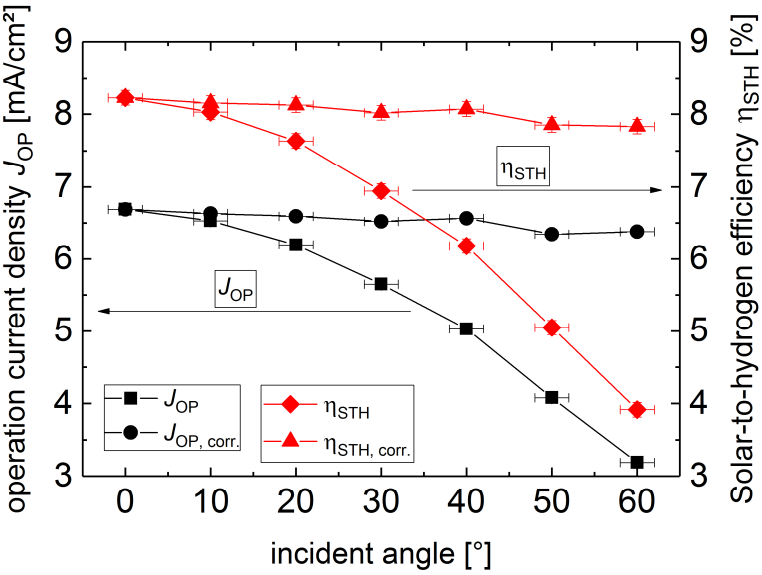


Figure 6: Evaluated operation current density $J_{OP}$ and STH efficiency $\eta_{STH}$ presented as a function of of the incident angle. The PV-EC systems consists of an a-Si:H/a-Si:H/µc-Si:H solar cell and Pt/$IrO_X$ catalysts. The data shown by black circles and red triangles correspond to the case when the area was corrected according to cosine law [3].

***Evaluation of long term $H_2$ production for various types of PV systems***

This part addresses an evaluation of long-term performance and $H_2$ production in PV-EC systems using various types of solar cells. Four types of solar cells (two junctions tandem, three junctions triple solar cells of two types and four junctions quadruple solar cells[5,39]) are studied and related with respect to long term H2 production under varied incident illumination. Considering potential effects of varied illumination on the system functionality, it is assumed that an a-Si:H/a-Si:H/µc-Si:H solar cell [23–25] and the solar cells of other types studied here demonstrate similar trends with respect to the effects of illumination intensity , variations in the temperature and angle. Therefore, the PV-EC systems based on various types of solar cells studied here are determined by the changes in the spectral composition of the incident light, which then represent an upper limit. As an example, the strategy for the evaluation of long term $H_2$ production presented earlier is applied for the case of a PV-EC system utilizing a three-junction solar cell (consisting of a-Si:H/a-Si:H/µc-Si:H sub cells) integrated with EC catalyst pair of Pt and $IrO_x$ (used as HER and OER electrode respectively). The described evaluation procedure is also used for the integrated systems utilizing all types of solar cells. The calculations are made for the system size of 1 square meter.

For evaluation of the long term H2 generation, realistic outdoor spectral data, corresponding to a particular location, are taken from reference [15]. In the reported spectral data the highest irradiance number is given for an APE over the APE value of the AM1.5G illumination.[15] The J-V characteristics of the various types of solar cells investigated here were studied in the interval of average photon energy values between -0.26eV to +0.18 eV relative to AM1.5G.

*1. J-V characteristics measured under modified APE and standard AM 1.5G spectra*

The photovoltaic parameters obtained for the spectra with varied average photon energies are presented in Figure 7. The J-V characteristics obtained under the maximum and minimum APE spectra (achieved by adjusting the fraction of the incident light sources can be found in the supplementary information (Figure S6) (ΔAPE = 0.44 eV). The figures show that the open circuit voltage is in a range of 2.16V – 2.24 V. The highest $V_{OC}$ values are obtained for ΔAPEs in the range of -0.02 to +0.04 eV. The short circuit current density shows the highest values for ΔAPE =0 and ΔAPE =+0.02 eV and is reduced for all other spectral variations. The photovoltaic efficiency shows a clear maximum value for ΔAPE = +0.02 eV. The fill factor increases with increasing ΔAPE but does not show a clear trend. In all cases, standard test conditions were maintained (T=25 °C, light intensity of 1 kW/m²) and normal angle of illumination.

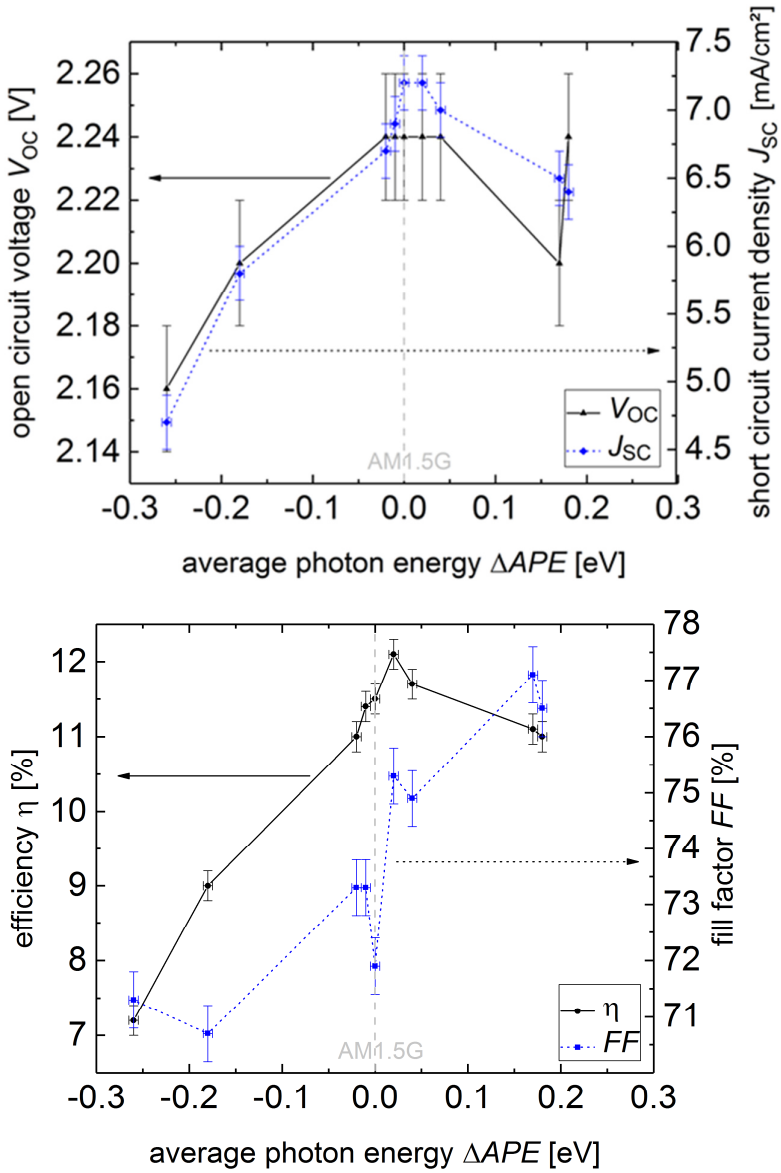


Figure 7: J-V characteristics of an a-Si:H/a-Si:H/µc-Si:H triple junction solar cell plotted versus the relative APE of the incident illumination spectrum, covering a range of 0.44eV (strongly red shifted to strongly blue shifted) (a) open circuit voltage (axis on the left hand side) and short circuit current density (axis on the right hand side) and (b) photovoltaic efficiency (left hand axis) and fill factor (right hand axis). Error bars calculated based on repeated measurements are shown.

*2. Evaluation of the STH efficiencies under modified APE and standard AM 1.5G spectra*

In order to evaluate the STH efficiency values under various spectral compositions studied here, the J-V characteristics of the solar cells were joined with J-V characteristics of the catalytic pair (Pt and $IrO_x$) according to the equivalent electrical circuit model (see above Experimental section). Figure 8 shows the calculated STH efficiency values presented as a function of difference APE (ΔAPE), which described the deviation in APE of a given spectral irradiance from the APE value of a standard AM1.5G illumination (ΔAPE=0 for the case of AM1.5G illumination). It can be seen that when ΔAPE values are negative, the STH efficiency decreases with lower ΔAPE. In the case of positive ΔAPE values, the STH shows a maximum value of around 8.4% at ΔAPE of $2x10^{-2}$ eV. When ΔAPE is above $2x10^{-2}$ eV, the STH efficiency is reduced and reach the value below 7.5%.

The procedure performed above was repeated for other types of solar cells studied here, the results are shown in the supplementary information (Figure S7 and S8).

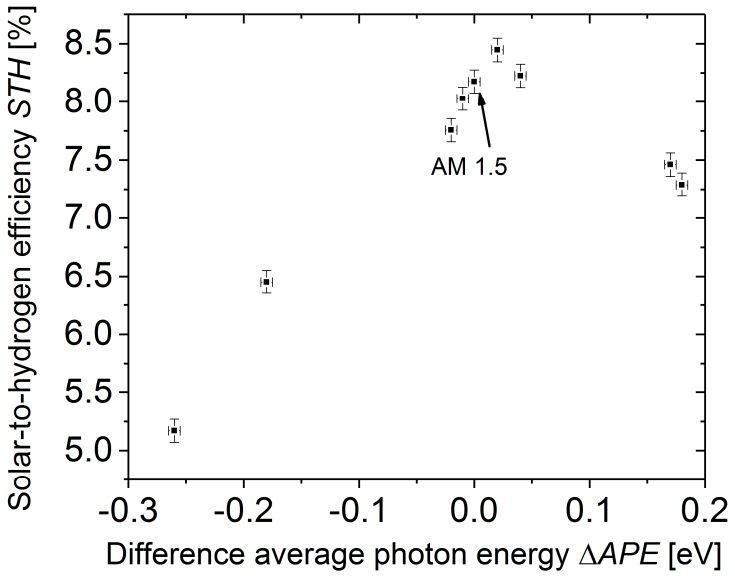


Figure 8: STH efficiency presented as a function of ΔAPE for the integrated PV-EC system based on triple junction (type a-Si:H/a-Si:H/µc-Si:H) solar cell and Pt/IrOx catalyst system.

*3. Reference spectral data as a function of APE*

Figure 9 presents reference annual irradiance obtained for a location in Shiga prefecture in Japan[15]. The data from ref. 15 was replotted in terms of ΔAPE where the standard AM1.5G illumination corresponds to zero ΔAPE. Note that the highest irradiance value is obtained for the positive ΔAPE (ΔAPE = $5x10^{-2}$ eV), indicating annual shift towards short wavelength region relative to the standard AM1.5G illumination. The experimental data was fitted using a Gaussian distribution presented by the red curve in Figure 9. The function [6] was used for the fitting with an RMS value of 0.99, using software Origin:

$$y = (10.3 \pm 3.0) + \frac{(8.8 \pm 0.4)}{((0.06 \pm 0.01) \cdot \sqrt{\frac{\pi}{4 \cdot \ln(2)}}} \cdot e^{\left(\frac{-4 \cdot \ln(2) \cdot (x-0.04)^2}{(0.06 \pm 0.01)^2}\right)} \quad [6]$$

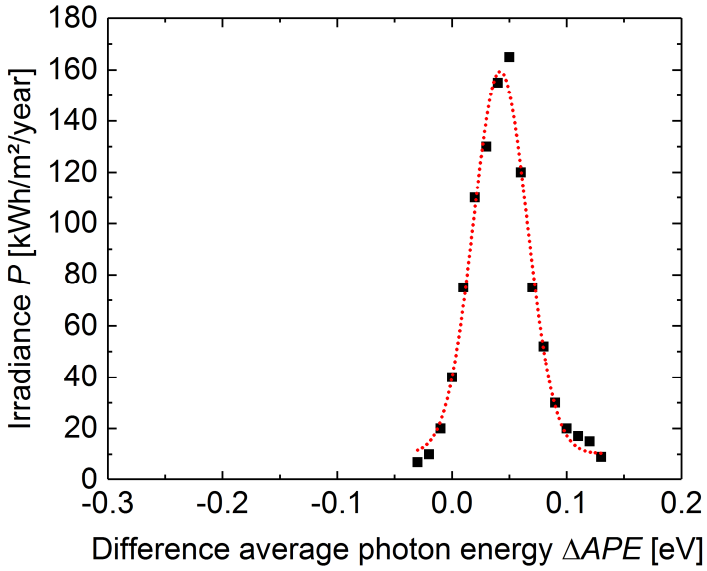


Figure 9: Reference annual irradiance P presented as a function of ΔAPE, replotted from the literature data for a location in Shiga prefecture in Japan [15]. Red line is a fitting curve obtained using function [6], see details in the text.

*4. Calculation of the annual irradiance using Gaussian fitted curve*

The ΔAPEs presented here (ΔAPE = $2x10^{-2}$ eV was adopted) are similar and in the range of ΔAPEs presented in earlier works (for example ΔAPE = $+1x10^{-2}$ eV and ΔAPE = $+3x10^{-2}$ eV were presented). In this work, the Gaussian fitted curve is adopted to define the annual irradiance at each relevant ΔAPE value required for the evaluation of STH efficiencies (total spectral intensity of 1 kW/m²). The STH values as a function of the average photon energy were convoluted with the corresponding ΔAPE.

*5. - 6. Evaluation of the total $H_2$ volume production*

In order to calculate the amount of hydrogen generated over a long term, the convoluted STH values over the studied interval of APE and the irradiance P were integrated to obtain the overall value. The result is multiplied by a coefficient defining the amount of $H_2$ produced at the STH of 1% (the coefficient is calculated as 2.5 L/m²). Equation 7 describes the calculation procedure. Additional details for these calculations and a comparison between the use of the experimentally obtained and the theoretically calculated factor, see the supplementary information (Figure S2 and S3).

$$V_{annual}(Hydrogen) = 1\ m^2 \cdot 2.5\ L/m^2 \cdot \int_{APE1}^{APE2} P(APE)\ \cdot\ STH(APE)\ dAPE \qquad [7]$$

Following eq 7, the calculated amount of $H_2$ produced over one year is shown in Figure 10. The X axis in the figure indicates various types of solar cells studied here.

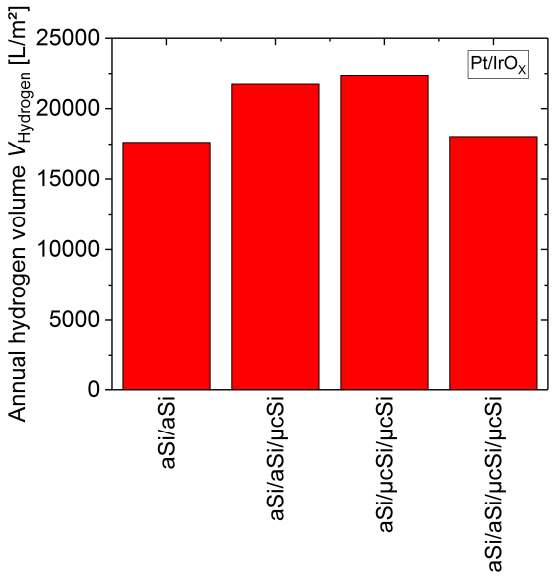


Figure 10: The amount of $H_2$ produced over one year by a PV-EC system with $Pt/IrO_x$ catalysts. The evaluation is performed for a reference annual irradiation data [15]

It can be seen in Figure 10 that implementation of a-Si:H/a-Si:H and a-Si:H/a-Si:H/µc-Si:H/µc-Si:H solar cells results in similar annual generation of $H_2$. Considering the solar cell manufacturing processes, a-Si:H/a-Si:H tandem devices are significantly simpler than a-Si:H/a-Si:H/µc-Si:H/µc-Si:H solar cells, thus the manufacturing of a more complex a-Si:H/a-Si:H/µc-Si:H/µc-Si:H photovoltaic structures would likely not be needed from the viewpoint of time consumption and material costs. The highest $H_2$ generation is observed for the case of an a-Si:H/µc-Si:H/µc-Si:H solar cell. The other triple junction solar cell (a-Si:H/a-Si:H/µc-Si:H) shows a little reduced annual $H_2$ volume compared to the champion device, however, the manufacturing process of a-Si:H/a-Si:H/µc-Si:H solar cells is less time consuming (and thus more cost efficient) compared to a-Si:H/µc-Si:H/µc-Si:H solar cells. Summarizing these observations, it is likely that a-Si:H/a-Si:H/µc-Si:H solar cells would be an optimal choice (in terms of manufacturing complexity and a produced amount of $H_2$) to be used in the integrated PV-EC systems for long term $H_2$ production.

Summary and Conclusions:

Regarding the influence of varied illumination angle, the PV-EC system studied in the present work (utilizing an a-Si:H/a-Si:H/µc-Si:H solar cell and a Pt/IrOx catalyst pair) can produce $H_2$ over the interval of incident angles up to 60°. A non-zero $J_{op}$ is obtained for the evaluated angular range, and therefore the $H_2$ generation is continuing at these angles. The decrease in the area of illumination, related to the angular effects is broadly similar to the effects of intensity reduction (decreased photon flux) following the geometric cosine rule. In this context, the changes in the incident angle form a secondary loss mechanism, that is combined with the essential losses in the number of photons. This results in decrease in the $H_2$ volume produced and deteriorations in the functionality of the system. It is important to note here that the angular effects and related reduction in the system functionality should be considered for the future PV-EC system designs to preferably maintain close to normal incidence conditions. This may also require additional considerations for the design of relevant parts (such as liquid or gas volumes) in the inclined states.

We evaluated the long term (1 year) generation of $H_2$ by a PV-EC device depending on the annual APE of the spectra available for a particular location. The performance of the PV-EC system and *STH* efficiency showed significant variation upon changes in the spectral composition (presented as a range of APE values). Exemplarily, we used reference annual solar irradiation data for a location in Shiga (Japan) and various thin film silicon based multi-junction as current-voltage sources, however the concept presented here can be applied to a wide range of various photoelectrodes, PV-EC devices and locations. Our model estimates the annual amount of around 20000 $L/m^2$ (ca. 2.25 $kg/m^2$) of hydrogen for the investigated triple junction solar cells depending on the variation of the spectral average photon energy for the given example. The results also suggest the importance to optimize the PV cell employed in the system with respect to the spectral variations found at the operation location rather than for laboratory conditions, allowing maximizing the volume of hydrogen produced.

Supporting Information

AM1.5G and modified spectra (Figure S1), STH and volume of the gas as a function of time (Figure S2), experimentally obtained and the theoretically calculated factors for the determination of the annual hydrogen volume (Figure S3), current density-voltage characteristics of the a-Si:H/a-Si:H/µc-Si:H solar cell under varied angles (Figure S4), current density-voltage curves for the PV-EC system under varied angles (Figure S5), current density-voltage characteristics of an a-Si:H/a-Si:H/µc-Si:H triple junction solar cell under modified spectra (Figure S6), J-V characteristics evaluated under modified spectra for various types of solar cells (Figure S7), STH as a function of ΔAPE (Figure S8)

Acknowledgment:

Partial financial support by the German Bundesministerium für Bildung und Forschung (BMBF) (network project: Sustainable Hydrogen (FKZ 03X3581A and FKZ 03X3581B)) and the Deutsche Forschungsgemeinschaft (DFG) (Priority Program 1613 (SPP 1613): Fuels Produced Regeneratively Through Light-Driven Water Splitting: Clarification of the Elemental Processes Involved and Prospects for Implementation in Technological Concepts) is gratefully acknowledged. We thank L. Ingenhorst for his support with setting up the measurement system, S. Dasgupta for his support with the measurements and helpful discussions, S. Kasper and C. Zahren for the assistance with measurements, S. Moll and H. Siekmann for their support with sample preparation.

Notes

The authors declare no competing financial interest.

References

[1] N. S. Lewis, Research opportunities to advance solar energy utilization, Science (80-. ).2016, 351, 353.

[2] A. C. Nielander, M. R. Shaner, K. M. Papadantonakis, S. A. Francis, N. S. Lewis, A taxonomy for solar fuels generators, Energy Environ. Sci. 2015, 8, 16–25.

[3] M. G. Walter, E. L. Warren, J. R. McKone, S. W. Boettcher, Q. Mi, E. A. Santori, N. S. Lewis, Solar Water Splitting Cells, Chem. Rev. 2010, 110, 6446–6473.

[4] C. C. L. McCrory, S. Jung, I. M. Ferrer, S. Chatman, J. C. Peters, T. F. Jaramillo, Benchmarking Hydrogen Evolving Reaction and Oxygen Evolving Reaction Electrocatalysts for Solar Water Splitting Devices, J. Am. Chem. Soc. 2015, 137, 4347–4357.

[5] F. Urbain, V. Smirnov, J.-P. Becker, A. Lambertz, F. Yang, J. Ziegler, B. Kaiser, W. Jaegermann, U. Rau, F. Finger, Multijunction Si photocathodes with tunable photovoltages from 2.0 V to 2.8 V for light induced water splitting, Energy Environ. Sci. 2016, 9, 145.

[6] F. Urbain, V. Smirnov, J.-P. Becker, U. Rau, F. Finger, J. Ziegler, B. Kaiser, W. Jaegermann, a-Si:H/μc-Si:H tandem junction based photocathodes with high open-circuit voltage for efficient hydrogen production, J. Mater. Res. 2014, 29, 2605–2614.

[7] F. Urbain, K. Wilken, V. Smirnov, O. Astakhov, A. Lambertz, J.-P. Becker, U. Rau, J. Ziegler, B. Kaiser, W. Jaegermann, et al., Development of Thin Film Amorphous Silicon Tandem Junction Based Photocathodes Providing High Open-Circuit Voltages for Hydrogen Production, Int. J. Photoenergy 2014, 2014, 249317.

[8] S. Zhang, L. Shen, T. Ye, K. Kong, H. Ye, H. Ding, Y. Hu, J. Hua, Noble-Metal-Free Perovskite–BiVO4 Tandem Device with Simple Preparation Method for Unassisted Solar Water Splitting, Energy Fuels 2020, 34, 4, 5016–5023

[9] Y. Cao, X. Zhu, J. Jianga, C. Liu, J. Zhou, J. Ni, J. Zhang, J. Pang, tational design of charge carrier transport layers for optimal antimony trisulfide solar cells and its integration in tandem devices, Solar Energy Materials and Solar Cells 2020, 206, 110279

[10] H. Xiao, P. Liu, W. Wang, R. Ran, W Zhou, and Z. Shao, Ruddlesden–Popper Perovskite Oxides for Photocatalysis-Based Water Splitting and Wastewater Treatment, Energy Fuels 2020, 34, 8, 9208–9221

[11] F. Urbain, V. Smirnov, J.P. Becker, A. Lambertz, U. Rau, F. Finger, Light-induced degradation of adapted quadruple junction thin film silicon solar cells for photoelectrochemical water splitting, Solar Energy Materials and Solar Cells 2016, 145, 142-147

[12] M.A. Muñoz-García, O. Marin, M.C. Alonso-García, F. Chenlo, Characterization of thin film PV modules under standard test conditions: Results of indoor and outdoor measurements and the effects of sunlight exposure, Solar Energy 2012 86, 3049-3056

[13] J. W. Ager, M. R. Shaner, K. A. Walczak, I. D. Sharp, S. Ardo, Experimental demonstrations of spontaneous, solar-driven photoelectrochemical water splitting, Energy Environ. Sci. 2015, 8, 2811–2824.

[14] Z. Chen, T. F. Jaramillo, T.G. Deutsch, A. Kleiman-Shwarsctein, A. J. Forman, R. Garland, Accelerating materials development for photoelectrochemical hydrogen production: Standards for methods, definitions, and reporting protocols, J. Mater. Res. 2010, 25, 3–16.

[15] T. Minemoto, S. Nagae, H. Takakura, Impact of spectral irradiance distribution and temperature on the outdoor performance of amorphous Si photovoltaic modules, Sol. Energy Mater. Sol. Cells 2007, 91, 919–923.

[16] C. Cornaro, A. Andreotti, Influence of Average Photon Energy index on solar irradiance characteristics and outdoor performance of photovoltaic modules, Prog. Photovolt Res. Appl.2013, 21, 996–1003.

[17] T. Minemoto, S. Fukushige, H. Takakura, Difference in the outdoor performance of bulk and thin-film silicon-based photovoltaic modules, Sol. Energy Mater. Sol. Cells 2009, 93, 1062–1065.

[18] S. Nagae, M. Toda, T. Minemoto, H. Takakura, Y. Hamakawa, Evaluation of the impact of solar spectrum and temperature variations on output power of silicon-based photovoltaic modules, Sol. Energy Mater. Sol. Cells 2006, 90, 3568–3575.

[19] L. Mutiara, K. Pegels, A. Reinders, valuation of spectrally dis-tributed irradiance in The Netherlands regarding the energy performanceof various PV technologies, Proc. IEEE 42nd Photovolt. Spec. Conf.2015.

[20] S. N. Agbo, T. Merdzhanova, U. Rau, O. Astakhov, Illumination intensity and spectrum-dependent performance of thin-film silicon single and multijunction solar cells, Sol. Energy Mater. Sol. Cells 2017, 159, 427–434.

[21] R. Gottschalg, D. G. Infield, M. J. Kearney, Experimental study of variations of the solar spectrum of relevance to thin film solar cells, Sol. Energy Mater. Sol. Cells 2003, 79, 527–537.

[22] R. Gottschalg, T. R. Betts, D. G. Infield, M. J. Kearney, On the importance of considering the incident spectrum when measuring the outdoor performance of amorphous silicon photovoltaic devices, Meas. Sci. Technol. 2004, 15, 460–466.

[23] F. Urbain, J.-P. Becker, V. Smirnov, J. Ziegler, F. Yang, B. Kaiser, W. Jaegermann, S. Hoch, A. Maljusch, U. Rau, et al., Influence of the operating temperature on the performance of silicon based photoelectrochemical devices for water splitting, Mater. Sci. Semicond. Process. 2016, 42, 142–146.

[24] K. Welter, V. Smirnov, J.-P. Becker, P. Borowski, S. Hoch, A. Maljusch, W. Jaegermann, F. Finger, The Influence of Operation Temperature and Variations of the Illumination on the Performance of Integrated Photoelectrochemical Water-Splitting Devices, ChemElectroChem2017, 4, 2099–2108.

[25] V. Smirnov, K. Welter, J. Becker, F. Urbain, W. Jaegermann, F. Finger, The Effect of the Illumination Intensity on the Performance of Si Multijunction based Integrated Photoelectrochemical water Splitting Devices, Energy Procedia 2016, 102, 36–42.

[26] F. Urbain, V. Smirnov, J.-P. Becker, U. Rau, J. Ziegler, B. Kaiser, W. Jaegermann, F. Finger, Application and modeling of an integrated amorphous silicon tandem based device for solar water splitting, Sol. Energy Mater. Sol. Cells 2015, 140, 275–280.

[27] J.-P. Becker, F. Urbain, V. Smirnov, U. Rau, J. Ziegler, B. Kaiser, W. Jaegermann, F. Finger, Modeling and practical realization of thin film silicon-based integrated solar water splitting devices, Phys. status solidi A 2016, 213, 1738–1746.

[28] S. Reynolds, V. Smirnov, Modelling performance of two- and four-terminal thin-film silicon tandem solar cells under varying spectral conditions, Energy Procedia2015, 84, 251–260.

[29] J. Ziegler, B. Kaiser, W. Jaegermann, F. Urbain, J. P. Becker, V. Smirnov, F. Finger, Photoelectrochemical and Photovoltaic Characteristics of Amorphous-Silicon-Based Tandem Cells as Photocathodes for Water Splitting, ChemPhysChem 2014, 15, 4026–4031.

[30] W. Böttler, V. Smirnov, J. Hüpkes, F. Finger, Texture-etched ZnO as a versatile base for optical back reflectors with well-designed surface morphologies for application in thin film solar cells, Phys. status solidi A 2012, 209, 1144–1149.

[31] K. Wilken, Low Temperature Thin-Film Silicon Solar Cells on Flexible Plastic Substrates (PhD Thesis), in Schriften des Forschungszentrum Jülich, Energy & Environment, 2017, 377, ISBN 978-3-95806-235-1.

[32] K. Wilken, U. W. Paetzold, M. Meier, M. Smeets, N. Prager, M. Fahland, F. Finger, V. Smirnov, Light Management in Flexible Thin-Film Solar Cells—The Role of Nanoimprinted Textures and Tilted Surfaces, IEEE J. Photovoltaics 2015, 5, 1646–1653.

[33] J.-P. Becker, B. Turan, V. Smirnov, K. Welter, F. Urbain, J. Wolff, S. Haas, F. Finger, A modular device for large area integrated photoelectrochemical water-splitting as a versatile tool to evaluate photoabsorbers and catalysts, J. Mater. Chem. A 2017, 5, 4818.

[34] D. Abou-Ras, T. Kirchartz, U. Rau, Advanced Characterization Techniques for Thin Film Solar Cells, Wiley VCH, Weinheim, Germany, 2011.

[35] J. Nelson, The Physics of Solar Cells, Imperial College Press, London, 2003.

[36] I. A. Yunaz, S. Kasashima, S. Inthisang, T. Krajangsang, S. Miyajima, A. Yamada, M. Konagai, Effect of light intensity on performance of silicon-based thin film solar cells, Proc. IEEE 34th Photovolt. Spec. Conf. 2009, 153–157.

[37] S. Kasashima, R. Uzawa, B. Janthong, S. Inthisang, T. Krajangsang, P. Sichanugrist, M. Konagai, Performance of multi-junction silicon-based thin film solar cells under concentrated sunlight, Proc. IEEE 37th Photovolt. Spec. Conf. 2011, 634–637.

[38] F. Urbain, V. Smirnov, J. Becker, U. Rau, J. Ziegler, B. Kaiser, W. Jaegermann, F. Finger, Application and modeling of an integrated amorphous silicon tandem based device for solar water splitting, Sol. Energy Mater. Sol. Cells 2015, 140, 275–280.

[39] F. Urbain, Light induced water splitting using multijunction thin film silicon solar cells, in Schriften des Forschungszentrum Jülich, Energy & Environment, 2016, 323, ISBN 978-3-95806-148-4 ISBN 978-3-95806-148-4.

TOC Graphic

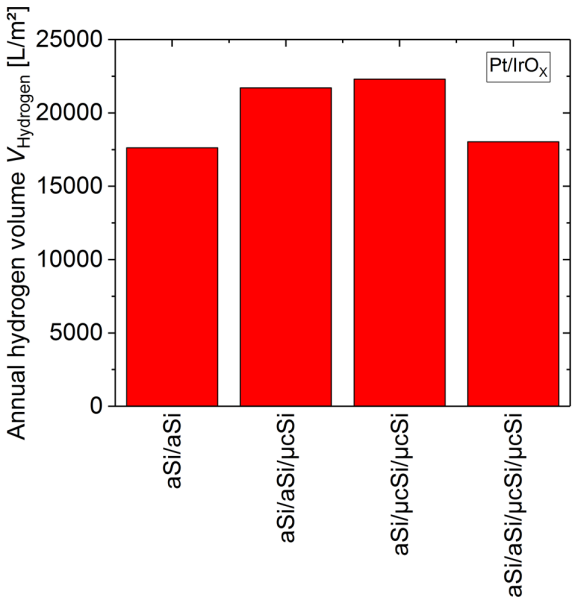
Annual hydrogen volume $V_{Hydrogen}$ [L/m²]
25000
20000
15000
10000
5000
0
Pt/IrO$_X$
aSi/aSi
aSi/aSi/µcSi
aSi/µcSi/µcSi
aSi/aSi/µcSi/µcSi